Available online at www.sciencedirect.com

ScienceDirect

Advances in Space Research xxx (2020) xxx–xxx

ADVANCES IN SPACE RESEARCH (a COSPAR publication)

www.elsevier.com/locate/asr

Adopting the empirical CODE orbit model to Galileo satellites

Dmitry Sidorov [a,*], Rolf Dach [a], Bernard Polle [b], Lars Prange [a], Adrian Jäggi [a]

[a] *Astronomical Institute of the University of Bern, Sidlerstr. 5, 3012 Bern, Switzerland*
[b] *Airbus Defence and Space, Rue des Cosmonautes 31, 31400 Toulouse, France*

Received 31 January 2020; received in revised form 15 April 2020; accepted 20 May 2020

Abstract

In 2012 the Center for Orbit Determination in Europe (CODE) joined the Multi-GNSS-EXtension project (MGEX) of the International GNSS Service (IGS). Since the end of 2013 the CODE MGEX contributions were based on combined solutions of five already established and emerging GNSS: GPS, GLONASS, Galileo, BeiDou and QZSS. This undertaking was made possible thanks to the continuous development of new models and approaches and their introduction in our processing schemes in order to ensure the delivery of products of the highest quality.

The European Galileo system with a total number of active satellites reaching the level of a nominal constellation is currently complete. Because of their relatively high area-to-mass ratio the Galileo spacecraft are more sensitive to non-gravitational forces than other GNSS satellites. The introduction of the extended empirical CODE orbit model (ECOM2) to the CODE MGEX solutions in early 2015 resulted in a significant improvement of the Galileo products. The use of the Galileo satellites metadata, which were made publicly available in the course of 2016 and 2017, has further enhanced the quality of the produced solutions. However, they still show significant degradations during eclipse seasons in particular for long-arc solutions (e.g., over three days), which are similarly observed in solutions of other IGS MGEX analysis centers to different extents. In particular this is reflected in elevated orbit misclosures, deterioration of the estimated satellite clock corrections and excessive satellite laser ranging (SLR) residuals during these periods. Since the ECOM2 parameters are designed to absorb the effect of solar radiation pressure, they are switched off during eclipses. Hence, there is no empirical force parameter left that can absorb any unmodelled perturbations (e.g., due to thermal radiation (TR)) during an eclipse period.

In this study we take advantage of the satellites' metadata to address the Galileo TR-induced accelerations and, therefore, to advance our orbit model further. By adjusting existing and introducing additional empirical parameters, as well as adopting a priori accelerations to account for unmodelled perturbations we achieve a significant improvement of our solutions. In particular, the use of a once-per-revolution sine term in the ECOM E_3 direction (satellite-Sun), activation of the constant term in the ECOM E_2 direction (along the solar panels) during the Earth's shadow transitions as well as the use of a priori acceleration in the body-fixed $+X$ direction substantially improve our solutions. The introduced modifications to the orbit model allow for an efficient adjustment of satellite velocity along the orbit that is necessary due to the apparent presence of unmodelled thermal radiation. The refinements lead to a substantial reduction of orbit misclosures and improvement of the radial orbital component accuracy during eclipse seasons up to 14% w.r.t. the solutions using ECOM2.

Keywords: Galileo; Non-conservative forces; Thermal radiation; Orbit modelling; Eclipse season; ECOM2

1. Introduction

For a long time, the American Global Positioning System (GPS) and its Russian counterpart GLObalnaya NAvigatsionnaya Sputnikovaya Sistema (GLONASS)

* Corresponding author.
E-mail address: dmitry.sidorov@aiub.unibe.ch (D. Sidorov).

https://doi.org/10.1016/j.asr.2020.05.028
0273-1177/

were the only two fully operational global navigation satellite systems (GNSS). However, with the number of active satellites reaching the level of a nominal constellation, the European GNSS Galileo is now complete and ready to provide additional reliability of the navigation services to its users (GSA, 2018a). By operating satellites that employ cutting edge technologies, Galileo is aimed to improve the supplied positioning and timing information (GSA, 2018b). This is done through the use of new signals and the advanced satellite payload that includes highly stable atomic frequency standards.

For the scientific community, the advent of the new GNSS implies the refinement of already developed solutions that support our understanding of geophysical processes of the Earth. This concerns a broad variety of fields, among which are, e.g., geodynamical studies, including the determination of terrestrial reference frames (Koivula et al., 2012; Nicolini and Caporali, 2018; Sośnica et al., 2018, 2019), as well as meteorological research (Benevides et al., 2017; Mendonca et al., 2018; Wang et al., 2018; Hoque et al., 2019; Wielgosz et al., 2019). Also, the data from Galileo satellites in eccentric orbits opened an opportunity for general relativity testing (Delva et al., 2018; Herrmann et al., 2018), for which the accuracy of satellite orbits and clock corrections is of high importance. Apart from this, the multi-GNSS analysis was shown to be beneficial in other fields, e.g., for precise time and frequency transfer (Zhang et al., 2018; Ge et al., 2019; Zhang et al., 2019).

In many cases, the applied multi-GNSS analysis relies on precise satellite products, i.e., orbits and satellite clock corrections. The International GNSS Service (IGS; Johnston et al., 2017), a voluntary federation of more than 200 institutions, is aimed to provide such products to the public on a regular basis. To pave the way towards the combined use of already established and emerging GNSS, the IGS started the Multi-GNSS Experiment (MGEX; Montenbruck et al., 2017) in 2011 and later renamed it to Multi-GNSS EXtension.

Galileo is one of the GNSS that is processed on a regular basis by various IGS analysis centers (ACs) within the frame of the MGEX project. As of 2019 the system consists of 4 In-Orbit Validation (IOV) satellites with one of them broadcasting on only one frequency and 21 Full Operational Capability (FOC) satellites, out of which 2 are in eccentric orbits (Sirikan et al., 2018). Thanks to the interest of station operators in the new systems as well as to the up-to-date support of receiver manufacturers, more than 290 permanent IGS stations provide Galileo data to the public (the IGS website[1]) as of August 2019. Due to the global distribution of these stations, the constellation is constantly well observed. This allows for achieving a rather high orbit quality among various IGS ACs. Montenbruck et al. (2018) reported that the Galileo orbits are consistent among different ACs within 10–20 cm (3D). A notable role in this achievement played the publication of the Galileo satellites' metadata by the European Global Navigation Satellite Systems Agency (GSA) over the course of 2016 and 2017 (GSA, 2019), which included information about the Galileo satellite dimensions, mass, surface optical properties, antenna phase center corrections and the attitude law. According to Prange et al. (2017b) and Dilssner et al. (2017), the use of these data resulted in a substantial improvement of Galileo precise orbit determination (POD).

The orbit modelling of Galileo satellites is challenging due to the relatively high area-to-mass ratio of these spacecraft ($0.012\ m^2/kg, 0.018\ m^2/kg$ and $0.019\ m^2/kg$ for GPS Block IIR, GPS Block IIF and Galileo satellites, respectively Schönemann et al., 2015). Also, the mass of each satellite is only around 700 kg, making them the lightest GNSS satellites orbiting the Earth. As a consequence, these spacecraft are more sensitive to non-conservative forces, among which solar radiation pressure (SRP), Earth's albedo, transmit antenna thrust and thermal radiation are the largest. As the orbit modelling techniques evolve, improving the orbit accuracy to a few centimeter, the subtle contribution of these forces becomes apparent, whereas their insufficient accounting may turn detrimental to the POD.

The Center for Orbit Determination in Europe (CODE) AC has been contributing with its product series (Prange et al., 2018) to MGEX since the beginning (Prange et al., 2017a). For SRP and other unaccounted non-gravitational force modelling, the Empirical CODE Orbit Model (ECOM; Beutler et al., 1994) was employed. By the model definition, the perturbing forces acting on a satellite in yaw attitude mode are decomposed into three orthogonal directions: satellite-Sun (E_3), along the solar

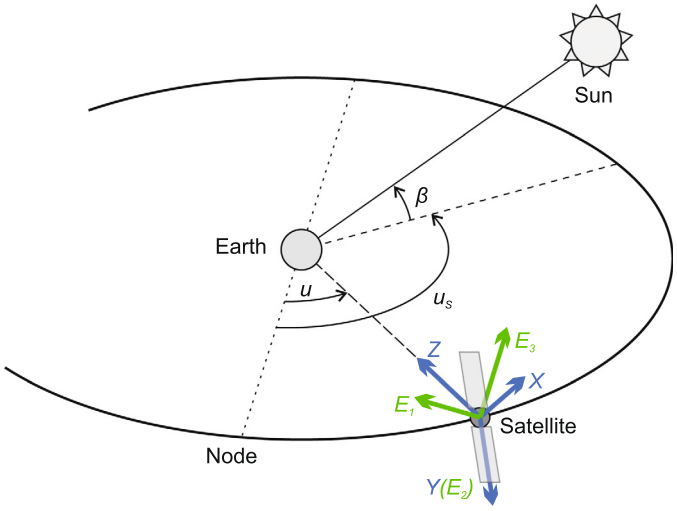

Fig. 1. Schematic representation of the body-fixed (XYZ) and the Sun-oriented ($E_3E_2E_1$) reference frames. u, u_S and β are arguments of latitude of the satellite and of the Sun and elevation of the latter above the orbital plane, respectively.

[1] http://www.igs.org, accessed on 23 August 2019.

Please cite this article as: D. Sidorov, et al., Adopting the empirical CODE orbit model to Galileo satellites, Advances in Space Research, https://doi.org/10.1016/j.asr.2020.05.028

panels (E_2) and the third direction (E_1) completing the right-handed system[2], Fig. 1. The modelled force in each direction is described by a constant and once-per-revolution sine and cosine functions of the argument of latitude of a satellite. The coefficients of these terms are empirically estimated as part of the orbit determination. Note that notations of the axis as well as of the parameters of the empirical models used in this study are consistent with Prange et al. (2020). According to this convention, the parameter name starts with the axis notation followed by zero for a constant term or by *Cku* or *Sku* for periodic functions of the argument of latitude of the satellite w.r.t. the Sun, Δu. *C* or *S* indicate if this is a cosine or sine function, respectively, whereas *k* stands for the argument multiplier.

Springer et al. (1999) suggested to update the model by removing periodic terms in E_3 and E_2 directions aiming to improve length-of-day (LOD) estimates. In such a configuration the ECOM was used within the IGS activities (including MGEX) at CODE until the model update in early 2015. In order to better account for the elongated structure of GLONASS satellites and of other emerging GNSS, ECOM2 was developed (Arnold et al., 2015), leading to the introduction of twice- (E_3S2u and E_3C2u) and four times per revolution (E_3S4u, E_3C4u) periodic terms in the E_3 direction. Also, the argument of latitude of a satellite was replaced by that w.r.t. the Sun. The E_3S4u and E_3C4u terms were constrained in June 2015, as they deteriorated the computed GLONASS solutions (Dach et al., 2016).

The introduction of ECOM2 in the frame of the MGEX processing at CODE AC resulted in a significant improvement of the Galileo products (Prange et al., 2017a). A significant contribution to this assessment was made by the International Laser Ranging Service (ILRS; Pearlman et al., 2002). According to the analysis of the satellite laser ranging (SLR) residuals, the Galileo products' β-angle (elevation of the Sun w.r.t. the orbital plane) dependency was considerably reduced compared to the ECOM-computed results. Additionally, this change led to enhancements in the computed Galileo clock corrections expressed as RMS of linear clock fits. This represented the state-of-the-art in the Galileo orbit modelling at the CODE AC, on which this study builds up.

Followed by the motivation of the current study, the consecutive sections provide derivations of the empirical model update for Galileo based on the published satellite metadata as well as the analysis of already computed CODE MGEX solutions. The benefits from the use of the updated empirical model compared to ECOM2 during eclipse seasons are discussed in the results section. The last section draws conclusions of the current study.

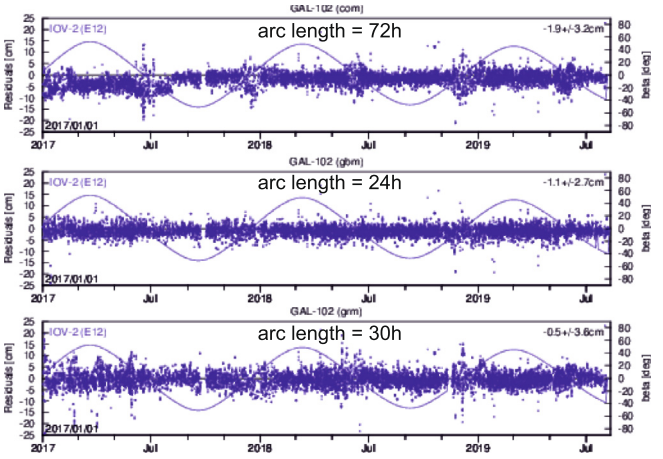

Fig. 2. SLR residuals of E12 orbits by (listed from the top of figure) CODE, GFZ and CNES/CLS ACs. MGEX Product Analysis web-page. Accessed on 23 August 2019.

2. Motivation

Although making use of the ECOM2 together with the satellite metadata information significantly improved the produced Galileo solutions, they are still degraded during eclipse seasons (Prange et al., 2017b). The primary cause of this is the insufficient accounting for non-conservative forces while the β-angle is low and the employed orbit model becomes incapable of compensating for these effects. This results in poor orbit modelling as seen, e.g., in higher than usual RMS of multi-day orbital arc fits w.r.t. the original orbits, in elevated orbit misclosures, in increased scatter of SLR residuals, etc. This effect is amplified with the increase of the orbital arc length that is used to determine orbital parameters, indicating deficiencies of the employed orbit model. In particular, the Galileo modelling issues are almost not present in the CODE AC 1-day solutions, however, they become clearly visible when 3-day solutions are generated.

Compared to the validation of the legacy GPS/GLONASS products performed by the IGS, that of the Galileo orbits carried out in the frame of the MGEX is not as comprehensive. Nevertheless, it still provides valuable metrics to assess quality of solutions generated by different ACs. In particular, the SLR residuals provide an important insight into the accuracy of primarily the radial component of the computed orbits. Fig. 2 depicts time-series of the one-way SLR residuals of E12 orbits provided by three ACs: CODE, GeoForschungsZentrum Potsdam (GFZ) and Centre National d'Etudes Spatiales and Collecte Localisation Satellites (CNES/CLS). The up-to-date time-series can be accessed on the MGEX product analysis web-page[3] of the IGS. At β-angles close to 0° the elevated scatter of the computed residuals can be observed in the solutions from the different ACs. Although the magnitude

[2] Formerly used axes notations are *D*, *Y* and *B* that correspond to E_3, E_2 and E_1, respectively.

[3] http://mgex.igs.org/analysis/index.php, accessed on 23 August 2019.

of the scatter for each AC is different, there is a correlation with the arc length used to produce the orbit solutions. The largest arc length of 72 h used at CODE corresponds to the largest scatter of the residuals at low β-angles. On the other hand, the scatter during eclipse periods using the GFZ solutions that employ 24 h arc length is not that prominent. The elevated scatter of the estimates during eclipse seasons suggests that multiple ACs have difficulties with modelling Galileo orbits at low β-angles.

Orbit misclosures at midnight (Lutz et al., 2016) are operationally monitored while performing POD at CODE AC. Excessive values of the misclosures may indicate deficiencies in orbit modelling. Thus, May-July 2019 were marked by eclipse seasons for two Galileo orbital planes affecting altogether 15 satellites. During days 134–168 spacecraft having pseudo-random noise (PRN) codes E11, E12, E13, E15, E26, E33 and E36 were in eclipse and during days 162–193 those having PRNs E01, E02, E21, E24, E25, E27, E30 and E31 were crossing the Earth's shadow. Fig. 3 shows three-dimensional orbit misclosures of Galileo satellites estimated during days 130–200 of 2019 using the development version of the Bernese GNSS Software (BSW; Dach et al., 2015). The employed POD procedure was identical to the one used for the MGEX product generation at CODE. The deficiencies of the employed orbit modelling, i.e., the use of the 7-parameter ECOM2, resulted in elevated orbit misclosures during eclipse seasons.

The Galileo satellites have two rubidium atomic frequency standards (RAFS) and two passive hydrogen masers (PHM) onboard. The payload of most of the Galileo satellites runs on PHM that have been assessed by high stability in various studies (Prange et al., 2017a; Steigenberger and Montenbruck, 2017; Huang et al., 2019). Taking into account the stability of the Galileo clocks, the evaluation of the estimated satellite clock corrections represented by a linear fit can therefore serve as an additional indicator of the radial orbit accuracy. Fig. 4 shows the RMS of the linear fit of the estimated clock corrections for E01 during one eclipse season. During

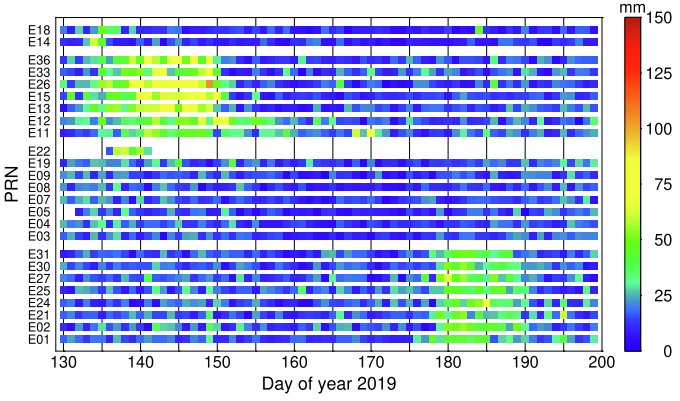

Fig. 3. Three-dimensional orbit misclosures of Galileo satellites employing ECOM2 over days 130–199 of 2019. The satellites are grouped by orbital planes.

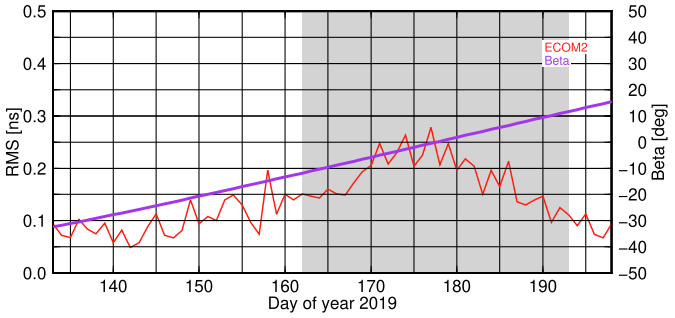

Fig. 4. RMS of linear clock fit of E01 estimated over days 133–199 of 2019. The shaded area indicates the eclipse season.

this period the satellite payload was operating on PHM, which is confirmed by the low estimated RMS of linear clock fit outside of eclipse season. During the eclipse seasons the estimated RMS is increased, suggesting unaccounted change of the radial orbital component. The similarly shaped, but even more pronounced bump in the clock fit RMS during eclipse seasons for Galileo was observed by Prange et al. (2017a) after the switch to ECOM2. Note that in contrast to the work of Prange et al. (2017a), the current study employs stochastic orbital parameters (Beutler et al., 1994), i.e., instantaneous satellite velocity changes every 12 h (at noon and midnight). These so-called pseudo-stochastic pulses are aimed to absorb effects not accounted by the specified orbit model. In turn, they may be very efficient in compensating some of the unmodelled effects (e.g., thermal radiation), thus, improving the solutions. In official CODE MGEX solutions the pseudo-stochastic pulses for Galileo were activated on August, 14 2017 (Dach et al., 2018). In accordance with that the stochastic pulses in the current study were set up for Galileo satellites in the radial, along-track and out-of-plane directions every 12 h. To a large extent, this explains the lower RMS of linear clock fits of Galileo satellites during their eclipse seasons compared to solutions of Prange et al. (2017a). However, the results clearly indicate the presence of orbit modelling deficiencies at low β-angles for these spacecraft.

3. Theoretical aspects

The detailed metadata package published by the GSA contains valuable details about the surface properties of the Galileo satellites. Of particular interest are thermal radiators that are installed on various surfaces of Galileo IOV and FOC satellites. Thermal radiators on satellites are designed for efficient evacuation of excessive heat from the payload to space through radiation. As any other source of radiation, thermal radiation (TR) creates a force applied to the radiating body. Thus, according to Lambert's law, the TR is diffused, creating a force

$$\mathbf{F}_t = -\frac{2}{3}\frac{\sigma}{c}\varepsilon T_a^4 A \hat{\mathbf{n}}_a \quad (1)$$

Please cite this article as: D. Sidorov, et al., Adopting the empirical CODE orbit model to Galileo satellites, Advances in Space Research, https://doi.org/10.1016/j.asr.2020.05.028

that depends on ε, T_a and A being the radiator emissivity, temperature and area, respectively, whereas σ is the Stefan–Boltzmann constant and c is speed of light. The force is pointing into the opposite direction than the surface normal vector $\hat{\mathbf{n}}_a$.

For each spacecraft surface being in thermal balance, one may write the following steady state equation:

$$q_{in} - q_{out} + q_{dissipated} = 0, \tag{2}$$

where q_{in} and q_{out} is the power absorbed and radiated, respectively, by this satellite face and $q_{dissipated}$ is the power that is generated by payload and that is dissipated to space. For a surface that is not exposed to external radiation (which is often the case for satellite thermal radiators), $q_{in} = 0$. Also, according to Stefan–Boltzmann's law, the power that is dissipated by a radiator is

$$q_{out} = \sigma \varepsilon A T_a^4. \tag{3}$$

Combining Eq. (2) and Eq. (3) and introducing T_a to Eq. (1) the expression for the force due to thermal radiation is simplified to

$$\mathbf{F}_t = -\frac{2}{3}\frac{q_{dissipated}}{c}\hat{\mathbf{n}}_a. \tag{4}$$

At this point it is necessary to clarify the body frame convention used in this study. Note that the manufacturer-defined body frames of Galileo satellites are different from the IGS-specific body frames (Montenbruck et al., 2015). To avoid confusion of the reader, the authors will stick to the IGS-agreed notations.

According to the information provided in the Galileo satellite metadata package, certain faces of the IOV and FOC satellites are equipped with thermal radiators (see Table 1). There are at least two aspects to consider while accounting for TR-induced accelerations acting on Galileo satellites. Firstly, the setup of the radiators on the satellite bus is asymmetric. Therefore, it is likely that the resulting thermal forces may not counterbalance each other. Secondly, the thermal control of the satellites is unknown to the public, therefore it is unclear how much power is radiated and when it is emitted from the radiators. In particular, it is difficult to predict the operating regime of the $-Z$ radiator on FOC satellites. The $-Z$ face of Galileo satellites is periodically illuminated by the Sun, making the operating mode of the radiator installed on this face convoluted. Because of this the $-Z$ radiator of FOC satellites is not considered in the frame of this study. As for the other radiators, we assume that the power dissipated from them remains constant over time to simplify our derivations.

The IOV and FOC satellites are equipped with radiators mounted on the $-X$ face of the satellite body. Unlike the $+X$ face, the $-X$ is never illuminated by the Sun, justifying the positioning of the radiator. Next to this radiator the clock modules are located (Ventura-Traveset, 2017). Assuming that the clocks always operate, generating heat, there is likely constant power emitted by the radiator. In turn, this creates a constant acceleration in the satellite $+X$ direction independently on the location of the satellite in orbit. The power consumption of a RAFS module is in the order of 35 W (Jeanmaire et al., 1999), whereas the consumption of a PHM is expected to be in the range between 60 W (Mattioni et al., 2002) and 76 W (Rochat and Gioia, 2016). By adopting the maximum values, the total power consumed by the clocks is around 222 W. Thus, this power is likely to be dissipated by the $-X$ radiator if no other equipment requires cooling using the same radiator. In turn, assuming that no energy (or its amount is small and can be neglected) is coming to the radiator from the Earth, the associated force can be computed using Eq. (4).

We simulated the accelerations acting on a Galileo satellite due to the constant thermal emissions through the $-X$ radiator. The true attitude modelling does not significantly affect results of these simulations, therefore we used a simplified yaw attitude modelling. Due to the satellite attitude law, the associated force acts only in the along-track and out-of-plane directions. However, since at low β-angles the force mostly acts in the satellite along-track direction, while the out-of-plane component stays nearly unaffected, we are primarily focused on the along-track constituent. Fig. 5 shows the simulated accelerations in the satellite along-track direction depending on the β-angle and argument of latitude of the satellite w.r.t. that of the Sun, Δu. At low β-angles the accelerations are cyclic, leading to periodic increase and decrease of the satellite acceleration. When projected into the Sun-oriented system ($E_3E_2E_1$), the force mainly acts in the E_3 direction. Projections of

Table 1
Total surface areas of satellite bus faces and the corresponding radiators of Galieo IOV and FOC satellites. All values are given in [m^2]. The IGS notations are used for axis definitions.

Axis	IOV		FOC	
	face	radiator	face	radiator
$-X$	1.32	0.78	1.32	0.88
$+X$	1.32	–	1.32	–
$-Y$	3.00	2.00	2.78	1.65
$+Y$	3.00	1.97	2.78	1.54
$-Z$	3.00	–	3.04	0.96
$+Z$	3.00	–	3.04	–

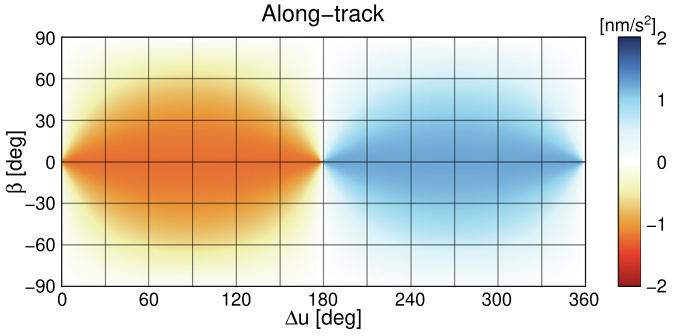

Fig. 5. Simulated accelerations in the along-track directions of Galileo satellites due to energy dissipation through the $-X$ radiator.

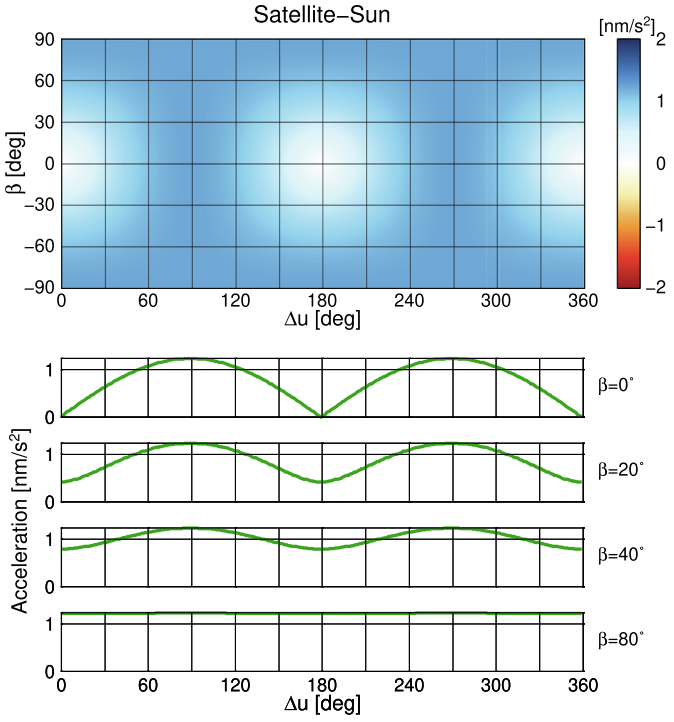

Fig. 6. Simulated accelerations in the satellite-Sun (E_3) directions of Galileo satellites due to energy dissipation through the $-X$ radiator. Acceleration profiles over one orbital revolution at β-angles of $0°, 20°, 40°$ and $80°$ are shown in the bottom.

the corresponding accelerations in the E_3 direction are shown in Fig. 6. While these accelerations at low β-angles are periodic, their profile changes with the increase of β-angle becoming more flat. At low β-angles this profile is such that the force cannot be fully taken into account by ECOM2 due to the model design. Besides, it is switched off during eclipses. However, as the direction of the thermal force is linked to a specific face of the satellite bus ($-X$), it can be modelled by introducing a constant acceleration in the body-fixed $+X$ direction equivalent to the assumed generated power. This approach has an advantage in reducing the load on empirical parameters with a side effect of lowering the risk of exchange among several parameters in absorbing such a force.

Keeping in mind the assumed dissipated power from the $-X$ radiator of 222 W, we performed tests in which we introduced a constant acceleration in the body-fixed $+X$ direction equivalent to a range of dissipated power values. By monitoring changes in the estimates of ECOM2 parameters as well as the SLR residuals to the computed orbits, we found that slightly higher than the assumed power values improve the solutions. Therefore, in our model we increased the assumed radiating power to 300 W, which the authors still regard as a reasonable value.

Instantaneous velocity changes, i.e., stochastic pulses are a valuable tool not only to absorb unmodelled forces, but also to analyze unaccounted forces that act on satellites. Similar to the CODE MGEX precise orbit solutions, in this study stochastic pulses were estimated every 12 h for Galileo satellites. Each time the pulses were estimated in three directions: radial, along-track and out-of-plane. The constraints of 1.0, 10 and 0.01 μm/s applied to the estimated stochastic pulses in the radial, along-track and out-of-plane components, respectively, were consistent with the official CODE MGEX solutions.

We have analyzed the time-series of the pulses for a set of eclipsing Galileo satellites. Noteworthy, the pulses in the along-track direction for these spacecraft follow a similar pattern, indicating additional accelerations of a satellite along the orbit, see Fig. 7. Such accelerations are observed for IOV (E11 and E12 in Fig. 7) as well as FOC satellites (E13, E15, E26, E33, E36 in Fig. 7). Note the discrepancy in behaviour of the estimated pulses for the IOV and FOC satellites reflecting the differences in satellite design. Interestingly, for the FOC satellites the magnitude of the pulses significantly reduces after the β-angle switches the sign. This may be related to variations of satellite attitude or its active thermal control before and after the middle of eclipse season.

In all observed cases the estimated stochastic pulses suggest the presence of a significant force that remains unaccounted by the employed ECOM2. There may be several reasons of such a force, e.g., heating up of certain surfaces of the satellite body and their cooling during the Earth's shadow transitions, active thermal control of a satellite during eclipse seasons, etc.

In an attempt to compensate for these velocity changes a once-per-revolution sine term in the E_3 direction (E_3S1u) was introduced in addition to other terms of ECOM2. At low β-angles the E_3S1u term acts mainly in the satellite along-track direction, reaching its maximum and minimum at $\Delta u = 90°$ and $\Delta u = 270°$, respectively, allowing for gradual change of the satellite velocity along the orbit. As the proposed term is aimed to compensate for the forces of non-SRP nature, it should remain active also during the Earth's shadow transitions.

There are several reasons why the introduced E_3S1u term is only active during eclipse seasons. Firstly, the aforementioned velocity adjustments are not necessary at higher β-angles. Secondly, the introduction of an additional

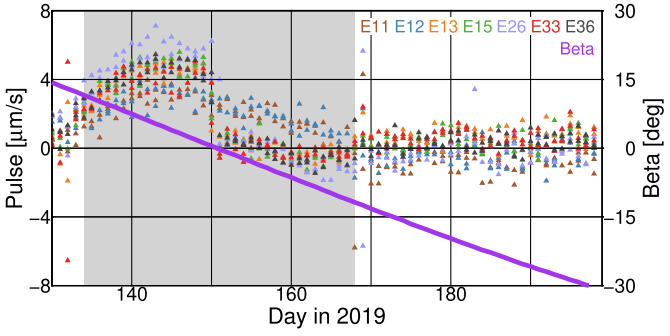

Fig. 7. Estimated stochastic pulses in the along-track direction for seven eclipsing Galileo satellites employing ECOM2 over days 130–199 of 2019. The shaded area indicates the eclipse season.

empirical parameter increases the risk of potentially high correlations with other parameters, leading to degradations of solutions.

Another refinement of the orbit model is related to the radiators installed on $+Y$ and $-Y$ faces of FOC satellites. The constant E_20 coefficient of ECOM2 is aimed to absorb forces along the satellite Y-axis (note that in yaw attitude mode E_2 matches the IGS Y direction in the satellite body-fixed frame). Such a force, namely the Y-bias (see, e.g., Fliegel et al., 1992; Springer et al., 1999), was observed for the GPS Block II/IIA satellites and was likely associated with mis-alignments of the satellite solar panels. A Y-bias was also present for the GPS Block IIR satellites and was probably related to the heat radiation from the satellite Y-panels (Marquis and Krier, 2000). A closer look at the time-series of the estimated ECOM2 E_20 parameter of the Galileo satellites, see Fig. 8, reveals the presence of a constant acceleration along the satellite Y-axis for the FOC satellites. At the same time, this effect seems to be almost not present for the IOV satellites. However, the metadata package describing the attitude of the Galileo FOC satellites does not report a potential mis-alignment of the solar array, therefore, the thermal nature of the force in the body-fixed Y-direction is likely the case for these spacecraft. This assumption is supported by the asymmetric sizes of the radiators installed on $+Y$ and $-Y$ faces of the FOC satellites (see Table 1). Thus, while the E_20 coefficient for the IOV satellites stays around 0 nm/s^2, the corresponding coefficient for the FOC satellites is estimated around -0.7 nm/s^2. Noteworthy, the estimates of E_20 coefficient are very consistent within each group of satellites. This leads to the assumption that the non-zero E_20 coefficient for the FOC spacecraft captures mostly the thermal force from the $+Y$ and $-Y$ radiators. Taking the non-SRP nature of the force, it is also reasonable to keep this coefficient active during the Earth's shadow transitions.

4. Model extensions w.r.t. ECOM2

In summary, the following set of modifications has been performed w.r.t. ECOM2 concerning the Galileo satellites:

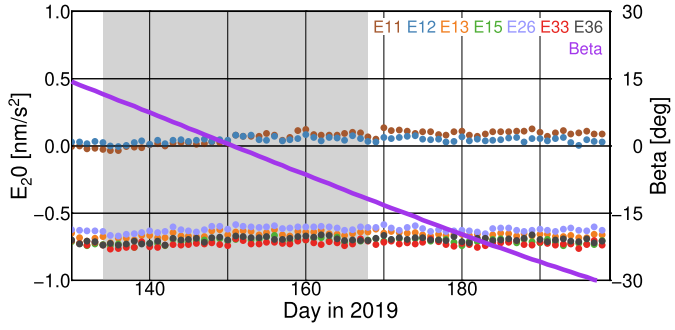

Fig. 8. The ECOM2 E_20 coefficient estimated for Galileo IOV (E11, E12) and FOC (E13, E15, E26, E33, E36) satellites during days 130–199 of 2019. The shaded area indicates the eclipse season.

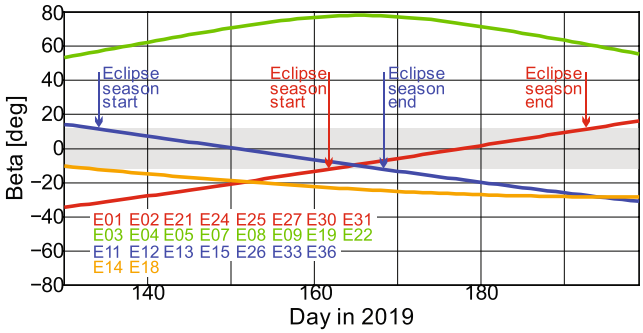

Fig. 9. Beta angles of Galileo satellites during days 130–199 of 2019. The shaded area indicates the eclipse condition. Start and end of eclipse seasons for two Galileo orbital planes are indicated.

- Introduction of an a priori acceleration in the satellite $+X$ direction equivalent to 300 W for all β-angles to compensate for the thermal emissions from the $-X$ radiators of Galileo satellites.
- Introduction of the once-per-revolution periodic term in the satellite-Sun direction (E_3S1u) for Galileo satellites during eclipse seasons to account for along-track accelerations potentially originating from other thermal effects during these periods. The E_3S1u term shall remain active also in the Earth's shadow due to the thermal nature of the associated forces.
- Activation of the E_20 term in eclipses for the Galileo FOC satellites, as the term primarily captures the thermal imbalance between the $+Y$ and $-Y$ faces of these spacecraft.

5. Analysis strategy

In order to highlight the advantages from the use of the updated orbit modelling for the Galileo satellites, a multi-GNSS processing involving 5 systems (GPS, GLONASS, Galileo, BeiDou and QZSS) was performed during days 130–199 of 2019. The processing setup was identical to the MGEX processing performed at CODE (Prange et al., 2018) with the only difference for the clock corrections generation: unlike in the official CODE clock solutions, no ambiguity resolution was performed. However, our tests suggest that keeping the ambiguities unresolved at their real values does not significantly change the results. Similarly to the CODE MGEX solutions, 3-day orbital arcs were generated in our POD procedure and the middle day was extracted. As a consequence, the use of the multi-day orbital arc solutions posed additional challenges to the orbit model under test.

Fig. 9 shows the β-angles of Galileo satellites during the aforementioned period. This time frame was selected because it covers two eclipse seasons for Galileo satellites (one during days 134–168 and another during days 162–193) and therefore is an excellent testbed for the refined model performance analysis. Both the IOV (PRNs E11

Please cite this article as: D. Sidorov, et al., Adopting the empirical CODE orbit model to Galileo satellites, Advances in Space Research, https://doi.org/10.1016/j.asr.2020.05.028

and E12) and the FOC (PRNs E01, E02, E13, E15, E21, E24, E25, E26, E27, E30, E31, E33 and E36) satellites are affected. Note that satellites with PRNs E14 and E18 placed in eccentric orbits were also used in processing with the same orbit modelling as the other FOC satellites.

Two sets of orbit and clock solutions were computed for the aforementioned period: one using ECOM2 and another using the extended ECOM2 for Galileo satellites as described in the previous section. Apart from the employed orbit model for Galileo satellites, no other differences were introduced in the setup of the two processing runs. The same development version of BSW was used in both cases.

6. Results

The proposed model changes for the Galileo satellites lead to a significant improvement of the orbit and clock solutions. The obtained results are thoroughly discussed in the following.

6.1. Orbit misclosures

As the poor orbit misclosures for the Galileo satellites during eclipse seasons were one of the motivating reasons to initiate this study, we start evaluating these quality indicators first. Fig. 10 shows orbit misclosures for Galileo satellites when the extended ECOM2 is employed. Although the multi-GNSS 5-system solution was computed, the other constellations are not shown here as the applied adjustments in orbit modelling did not have a significant impact on these GNSS. Compared to the solution using the original ECOM2 (Fig. 3), the proposed model changes flattened the orbit misclosures by reducing the peak values of over 70 mm to approx. 25 mm, bringing the values at low and high β-angles to the same level. The observed improvements are similar for the IOV and the FOC satellites.

Statistical values of orbit misclosures as well as velocity differences for the eclipsing Galileo satellites computed using ECOM2 and the extended ECOM2 are provided in Table 2. These combined data consider only eclipsing spacecraft during days 130–199 of 2019, highlighting the higher performance of the extended ECOM2. Noteworthy, the mean value of orbit misclosures over the two eclipse seasons was reduced by ~53%, reaching 13.9 mm using the extended ECOM2. Additionally, the estimated velocity differences were improved by ~42%, reaching 2.5 mm/s. The obtained values are well compared to that of other Galileo satellites being at high β-angles. The average numbers for them are around 14 mm and 2 mm/s for the position and velocity differences, respectively.

A careful reader may notice a few data points in solutions using extended ECOM2, notably in the beginning (around days 134 and 162) and end (around days 168 and 193) of eclipse seasons with slightly elevated values of orbit misclosures. These phenomena can be explained through the orbit model switch during these periods. In particular, the E_3S1u term is activated or deactivated around these days, leading to short-term inconsistencies in the orbit models used during consecutive days. Keeping in mind that this switch always occurs at midnight, slightly elevated orbit misclosures, in particular, in the along-track orbital component may be observed. By not considering the few data points with excessive values due to the activation and deactivation of E_3S1u, the values in Table 2 are further reduced. This indicates that the gradual along-track velocity adjustment of Galileo satellites during eclipse seasons by the use of the E_3S1u term was successful.

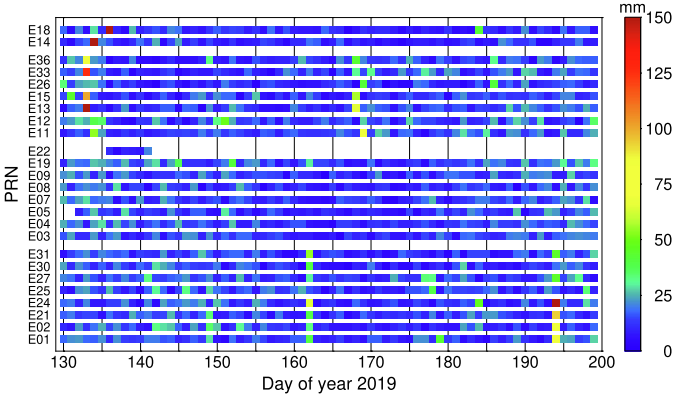

Fig. 10. Three-dimensional orbit misclosures of Galileo satellites employing the extended ECOM2 over days 130–199 of 2019. The satellites are grouped by orbital planes.

6.2. Stochastic pulses

Very promising results were obtained by analyzing stochastic pulses that were estimated every 12 h for Galileo satellites. The adjustments related to Galileo orbit modelling reduced the magnitudes of the along-track pulses during eclipse seasons to the values typical for higher β-angles (Fig. 11). The corresponding time-series outside and during eclipse season have become very similar, and, unlike in the solution using ECOM2 (see Fig. 7) showed no apparent pattern during eclipse seasons. Thus, the improvements are observed both in the mean as well as in the standard deviation of the stochastic pulses for each spacecraft. For the IOV satellites the mean along-track pulse is reduced from 2.0 ± 1.2 μm/s to 0.3 ± 1.0 μm/s,

Table 2
Statistical values of orbit misclosures and velocities differences of consecutive daily satellite arcs computed using ECOM2 and extended ECOM2. Only eclipsing Galileo satellites during days 130–199 of 2019 are considered. The units of positions and velocities are mm and mm/s, respectively.

Param.	Model	Mean	STD
Positions	ECOM2	29.3	19.0
	ext. ECOM2	13.9	12.6
Velocities	ECOM2	4.3	2.4
	ext. ECOM2	2.5	1.9

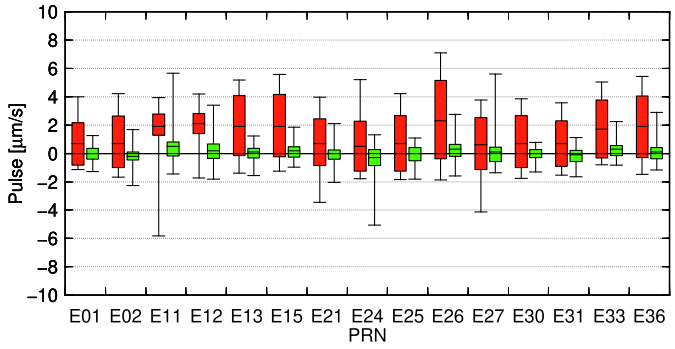

Fig. 11. Magnitude of stochastic pulses in the along-track direction for 15 Galileo satellites during two eclipse seasons over days 130–199 of 2019. Solutions computed using ECOM2 and extended ECOM2 are shown in red and green, respectively.

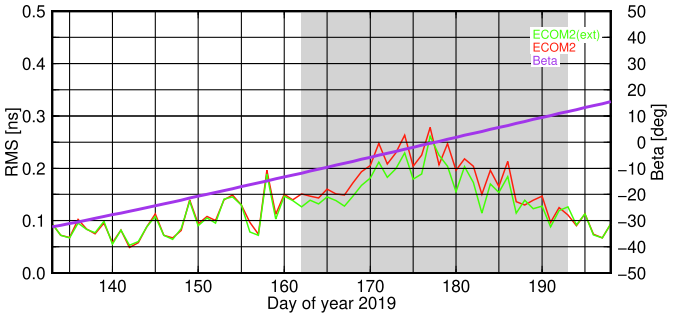

Fig. 12. RMS of linear clock fit of E01 using ECOM2 (red) and extended ECOM2 (green) estimated over days 133–199 of 2019. The shaded area indicates the eclipse season. (For interpretation of the references to colour in this figure legend, the reader is referred to the web version of this article.)

whereas for the FOC satellites the respective improvement is from 1.2 ± 2.2 µm/s to 0.0 ± 0.7 µm/s.

Although the estimated stochastic pulses for the Galileo satellites during eclipse seasons are greatly reduced with the mean approaching zero, our tests indicate that their use is still beneficial, as they provide fine adjustments to the computed orbits. The satellites may show slightly different behaviour due to subtle differences in surface properties or potential hardware malfunction, leading to the necessity of fine tuning of the applied orbit model. In turn, the stochastic pulses, if properly set up, may allow for further satellite-specific tailoring of the applied orbit model.

Fig. 11 highlights an important property of the stochastic pulses to absorb spacecraft-specific orbit modelling deficiencies. In particular, by looking at the solutions computed using ECOM2, the IOV satellites (E11 and E12) with very narrow distributions clustered around 2 µm/s can be easily identified. Besides, it appears that there are also distinctions in behaviour of various FOC satellites. For instance, E13, E15, E33 and E36 obviously belong to a group of satellites having common characteristics, as the stochastic pulses in the along-track component have similar distributions. It is interesting to note that these four FOC satellites are the newest spacecraft launched together on July 25 2018. At the same time, the other FOC satellites (except E26) behave differently, having the distributions of the along-track pulses more shifted towards zero. This suggests the presence of differences in the FOC satellite design, attitude or indicates other changes, e.g., in the spacecraft mass or surface properties. This, however, is beyond the scope of this study.

6.3. Satellite clock corrections

As the Galileo satellites operate highly stable PHM clocks, improvements due to the introduced orbit model change are also expected in the estimated satellite clock corrections. For this reason the satellite clock corrections of the solution using the extended ECOM2 were estimated and the linear clock fits were analyzed. Fig. 12 shows the RMS of linear clock fits estimated using the original and the refined empirical models. In eclipse season, when the E_3S1u term becomes active and the E_20 term is kept active for the FOC satellites, the improvements become apparent. It should be noted that according to the clock analysis, the introduced constant acceleration due to the $-X$ radiator does not result in a noticeable change outside eclipse season. At moderate β-angles the $-X$ radiator creates an acceleration that can be absorbed by the empirical E_3C2u term (see Fig. 6), therefore the contribution of the introduced constant acceleration becomes less visible.

The clock estimation results for all eclipsing Galileo satellites during days 130–199 of 2019 are summarized in Fig. 13. The fact that the mean as well as the scatter of the estimated RMS of linear clock fits are reduced for all considered satellites, provides another indication that the proposed refinements in orbit modelling improve the solutions. Taking the stability of the estimated clock corrections as an indicator of the computed radial orbit quality, it may be concluded that the use of the extended ECOM2 improves the respective component of the Galileo orbit solutions in eclipse seasons on average by 11%.

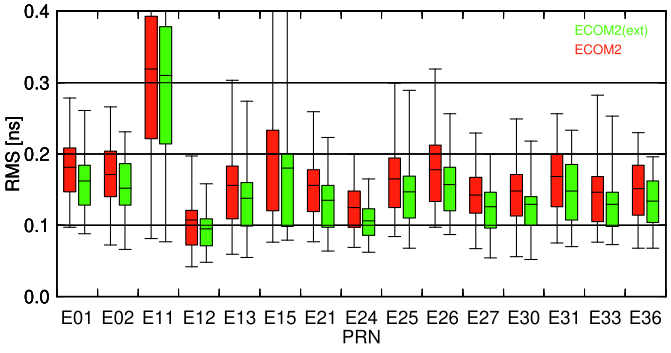

Fig. 13. Estimated linear clock fits for 15 Galileo satellites during two eclipse seasons over days 130–199 of 2019. Solutions computed using ECOM2 and extended ECOM2 are shown in red and green, respectively. (For interpretation of the references to colour in this figure legend, the reader is referred to the web version of this article.)

Please cite this article as: D. Sidorov, et al., Adopting the empirical CODE orbit model to Galileo satellites, Advances in Space Research, https://doi.org/10.1016/j.asr.2020.05.028

6.4. SLR residuals

Up to now the presented results were based on the evaluation of various parameters derived only from processing the GNSS data. In order to provide an independent evaluation of the computed orbit solutions, the one-way SLR residuals of the estimated Galileo orbits were evaluated. Fig. 14 shows histograms of the SLR residuals estimated for solutions using ECOM2 and the extended ECOM2. These results incorporate only the eclipsing Galileo satellites. The use of the extended ECOM2 results in a scatter of the SLR residuals reduced from 42.9 mm to 37.1mm. Thus, the observed improvement reaches approx. 14% w. r.t. the solution using ECOM2. This is in line with the improvements observed in the satellite clock corrections discussed above, as both metrics are directly related to the radial orbit accuracy.

While the scatter of the SLR residuals is reduced, the small mean SLR offset of −3.7 mm observed in the solution using ECOM2 was slightly increased and reached −4.5 mm. Noteworthy, both mean values are slightly shifted from the median values of −6.9 mm and −6.7 mm for the solutions using ECOM2 and extended ECOM2, respectively. Such a difference between the mean and median values is governed by wide tails of the distributions, whereas the change in the mean value in this particular case should not be regarded as an indication of poor orbit model performance. At the same time, the negative median offsets of both solutions may partly be due to the lack of SLR observations during daytime, since only eclipsing satellites are taken into account. However, other potential issues in this regard that directly contribute to the radial error budget, e.g, incorrect transmit power, inaccurate albedo modelling or errors in the satellite antenna Z-offset, etc., should not be neglected.

6.5. Correlations between the estimated parameters

It is well known that overparameterization of the empirical orbit model may introduce correlations between the estimated parameters, leading to degradations of solutions. For example, the use of once-per-revolution terms in E_3 in ECOM resulted in significant degradations of LOD (Springer et al., 1999). On the other hand, to support the extended ECOM2, the estimates of E_3S1u were very consistent across the eclipsed satellites of the same type (see below) and showed small formal errors. Nevertheless, for completeness the correlations among the estimated parameters were extracted from processing and analyzed.

Fig. 15 provides cross-correlations among the estimated osculating elements, empirical parameters of the orbit model of Galileo E01 and Earth orientation parameters (EOP) on day 176 of 2019. On this day this satellite was almost in the middle of its eclipse season, implying strong influence of the introduced E_3S1u parameter on other estimates. These results are part of the usual 3-day solution, where the middle day arc is extracted. The X and Y pole estimates are represented as offsets computed at noon and drifts over 1 day, whereas ΔUTC provides access to LOD. As can be seen, the correlations of E_3S1u with other empirical parameters as well as with the EOP are small. In order to check if the introduction of an additional empirical parameter changes correlations among other parameters of the empirical model, we compared this solution to another one in which the E_3S1u parameter was heavily constrained. The observed change in correlations among other parameters of ECOM2 due to the introduction of E_3S1u for the Galileo satellites was smaller than 1.5%. A similar picture is observed during other days when β-angle is low, suggesting the safe use of the new parameter in parameter estimation processes.

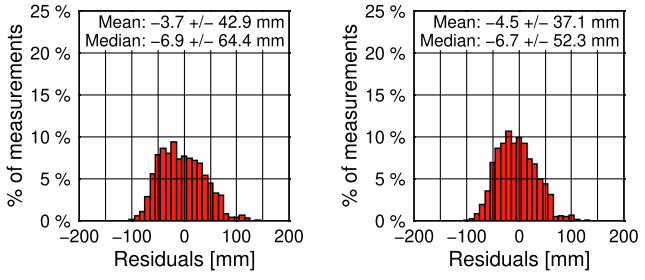

Fig. 14. Histograms of the estimated SLR residuals of Galileo satellite orbits using ECOM2 (left) and the extended ECOM2 (right). Only the eclipsing satellites over days 130–199 of 2019 have been considered. The mean and median values are provided together with standard deviations and interquartile ranges, respectively.

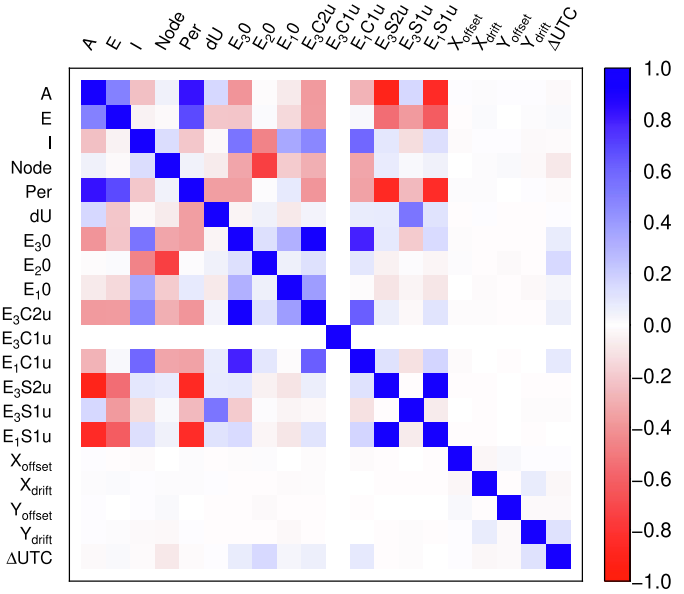

Fig. 15. Cross-correlations among 15 orbital parameters (6 osculating elements and 9 empirical orbit model parameters) of E01 and polar motion parameters estimated using a 3-day arc with a middle day on day 176 of 2019. β-angle is approx. −1.2°.

Please cite this article as: D. Sidorov, et al., Adopting the empirical CODE orbit model to Galileo satellites, Advances in Space Research, https://doi.org/10.1016/j.asr.2020.05.028

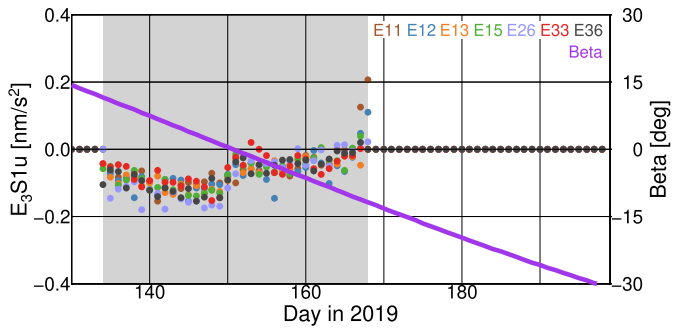

Fig. 16. The introduced E_3S1u coefficient estimated for Galileo IOV (E11, E12) and FOC (E13, E15, E26, E33, E36) satellites during days 130–199 of 2019. The shaded area indicates the eclipse season. Note that E_3S1u is only active during eclipse seasons.

6.6. Repeatability of the parameter estimates

As was shown above, the introduced E_3S1u parameter is very little correlated with other ECOM2 parameters. In turn, this suggests that the estimates of the new parameter should have good repeatability accompanied with little uncertainty. It is important to highlight that this parameter was unconstrained during the parameter estimation process.

The estimates of E_3S1u for two Galileo IOV and five FOC satellites during one eclipse season in May-June 2019 are shown in Fig. 16. Note that the E_3S1u parameter is only active during the eclipse season, therefore its estimates at $|\beta| > 11.9°$ are set to zero. During the eclipse season the parameter estimates usually stay between -0.2 nm/s^2 and 0 nm/s^2 for the Galileo satellites. In terms of orbital dynamics this introduces an acceleration that acts mainly in the satellite along-track direction.

As can be observed in Fig. 16, the magnitude of E_3S1u estimates reduces for the FOC satellites after β-angle changes the sign. This agrees with behaviour of the estimated stochastic pulses in the along-track direction (Fig. 7), as the last significantly reduce for the examined spacecraft after the middle of eclipse season. As mentioned previously, this is potentially related to changes in satellite attitude or its thermal control before and after the middle of eclipse seasons.

7. Conclusion

In this study we focused on non-conservative force modelling of Galileo satellites. Our investigations highlighted the high value of satellite metadata obtained from GSA to efficiently adjust orbit modelling strategies. In particular, based on the published satellite metadata we extended the ECOM2 to better account for non-SRP forces from the presence of thermal radiators on these spacecraft. The correct non-conservative force modelling for these lightweight satellites becomes fundamental in eclipse seasons because by design the ECOM2 parameters are unable to capture thermal forces that are still present in the Earth's shadow. The appropriate adjustments are necessary as the modelling deficiencies become apparent with extension of the orbital arc length.

The proposed modifications incorporate an a priori acceleration that is aimed to reduce the load on the empirical model, as well as adjustments of empirical parameters to account for non-conservative forces of non-SRP nature. The use of additional empirical terms is limited to low β-angles to reduce potential correlations with other estimated parameters as well as to minimize possible impact on global geodetic parameters, i.e., EOP and geocenter coordinate estimates.

Although the proposed modifications account for only a fraction of the thermal forces acting on the Galileo satellites, their use significantly improves the computed orbits, particularly, during eclipse seasons. Based on the analysis of the Galileo solutions computed over two eclipse seasons for these satellites in 2019, we observed improvements in results when this extended ECOM2 was in use. The evaluated metrics included orbit misclosures, instantaneous velocity changes, satellite clock corrections and SLR residuals. At the same time, estimates of the introduced once-per-revolution sine term in the satellite-Sun direction (E_3S1u) showed very good daily repeatability and small correlations with other parameters.

The authors pointed out that the abrupt midnight activation and deactivation of the E_3S1u term, as it was done in this study, may result in short-term orbit model inconsistency over consecutive days. In turn, this may lead to elevated orbit misclosures at the beginning and end of an eclipse season. To overcome this, a more gentle model switch may be implemented, involving a smooth constraining function for the E_3S1u coefficient.

Based on the obtained results the discussed model changes were introduced into CODE's precise GNSS product generation. In particular, the extended ECOM2 for Galileo was adopted for the MGEX products (Prange et al., 2018) and (Ultra-) Rapid products (Dach et al., 2019b,a) starting from GPS weeks 2054 and 2072, respectively.

The authors would like to emphasize that the assumptions presented in this study are based on the available satellite information as well as on the analysis of already computed POD solutions that indirectly suggest the presence of unmodelled thermal effects. While the adjustments in the orbit modelling considerably improved the computed Galileo orbit and clock corrections particularly during eclipse seasons, some orbit modelling deficiencies still persist. Apparently, these deficiencies stem from other unaccounted thermal forces that are not fully captured by the employed orbit model. These effects may be related to heating and cooling of satellite surfaces at low β-angles. The problem compounds by the presence of the thermal radiators on the $-Z$ face of the FOC satellite bus that is regularly illuminated by the Sun. Prediction of the operation mode of this radiator is challenging without knowledge of the satellite thermal control algorithms. Furthermore,

Please cite this article as: D. Sidorov, et al., Adopting the empirical CODE orbit model to Galileo satellites, Advances in Space Research, https://doi.org/10.1016/j.asr.2020.05.028

the time-series of the estimated E_3S1u coefficients (as well as the stochastic pulses) for the FOC satellites suggest a certain asymmetry in the satellite operation (e.g., attitude, active thermal control, etc.) w.r.t. the β-angle. Knowledge of these details will facilitate further advancing of the Galileo orbit modelling.

References

Arnold, D., Meindl, M., Beutler, G., Dach, R., Schaer, S., Lutz, S., Prange, L., Sośnica, K., Mervart, L., Jäggi, A., 2015. CODE's new solar radiation pressure model for GNSS orbit determination. J. Geodesy, 1–17. https://doi.org/10.1007/s00190-015-0814-4.

Benevides, P., Nico, G., Catalão, J., Miranda, P.M.A., 2017. Analysis of Galileo and GPS Integration for GNSS Tomography. IEEE Trans. Geosci. Remote Sens. 55, 1936–1943. https://doi.org/10.1109/TGRS.2016.2631449.

Beutler, G., Brockmann, E., Gurtner, W., Hugentobler, U., Mervart, L., Rothacher, M., Verdun, A., 1994. Extended orbit modeling techniques at the CODE processing center of the International GPS Service for Geodynamics (IGS): Theory and initial results. Manuscr. Geod. 19, 367–386.

Dach, R., Lutz, S., Walser, P., Fridez, P. (Eds.), 2015. Bernese GNSS Software Version 5.2. Astronomical Institute, University of Bern, Bern Open Publishing..

Dach, R., Schaer, S., Arnold, D., Orliac, E., Prange, L., Sidorov, D., Sušnik, A., Villiger, A., Jäggi, A., Beutler, G., Brockmann, E., Ineichen, D., Lutz, S., Wiget, A., Dostal, J., Thaller, D., Söhne, W., Bouman, J., Selmke, I., Hugentobler, U., 2018. Center for Orbit Determination in Europe (CODE) Technical Report. In: Villiger, A., Dach, R. (Eds.), International GNSS Service Technical Report 2017. University of Bern. IGS Central Bureau, Astronomical Institute.

Dach, R., Schaer, S., Arnold, D., Prange, L., Sidorov, D., Stebler, P., Villiger, A., Jäggi, A., 2019a. CODE rapid product series for the IGS. URL: http://www.aiub.unibe.ch/download/CODE, doi:10.7892/boris.75854.3. library Catalog: boris.unibe.ch Publisher: Astronomical Institute, University of Bern.

Dach, R., Schaer, S., Arnold, D., Prange, L., Sidorov, D., Stebler, P., Villiger, A., Jäggi, A., 2019b. CODE ultra-rapid product series for the IGS. URL: http://www.aiub.unibe.ch/download/CODE, http://dx.org/10.7892/boris.75676.3. library Catalog: boris.unibe.ch Place: Bern CHE Publisher: Astronomical Institute, University of Bern.

Dach, R., Schaer, S., Arnold, D., Orliac, E., Prange, L., Sušnik, A., Villiger, A., Maier, A., Mervart, L., Jäggi, A., Beutler, G., Brockmann, E., Ineichen, D., Lutz, S., Wiget, A., Rülke, A., Thaller, D., Habrich, H., Söhne, W., Ihde, J., Hugentobler, U., 2016. CODE Analysis Center Technical Report. In: Jean, Y., Dach, R. (Eds.), International GNSS Service Technical Report 2015. University of Bern. IGS Central Bureau, Astronomical Institute.

Delva, P., Puchades, N., Schönemann, E., Dilssner, F., Courde, C., Bertone, S., Gonzalez, F., Hees, A., Le Poncin-Lafitte, C., Meynadier, F., Prieto-Cerdeira, R., Sohet, B., Ventura-Traveset, J., Wolf, P., 2018. Gravitational Redshift Test Using Eccentric Galileo Satellites. Phys. Rev. Lett. 121, 231101. https://doi.org/10.1103/PhysRevLett.121.231101.

Dilssner, F., Schönemann, E., Springer, T., Flohrer, C., Enderle, W., 2017. Galileo Declassified: IOV Spacecraft Metadata and Its Impact on Precise Orbit Determination, in: EGU General Assembly Conference Abstracts, Vienna, Austria. p. 14378.

Fliegel, H.F., Gallini, T.E., Swift, E.R., 1992. Global positioning system radiation force model for geodetic applications. J. Geophys. Res.: Solid Earth (1978–2012) (97), 559–568. https://doi.org/10.1029/91JB02564/full.

Ge, Y., Dai, P., Qin, W., Yang, X., Zhou, F., Wang, S., Zhao, X., 2019. Performance of Multi-GNSS Precise Point Positioning Time and Frequency Transfer with Clock Modeling. Remote Sens. 11, 347. https://doi.org/10.3390/rs11030347.

GSA, 2018a. Galileo Initial Services. URL: https://www.gsa.europa.eu/galileo/services/initial-services.

GSA, 2018b. Galileo Services. URL: https://www.gsa.europa.eu/galileo/services.

GSA, 2019. Galileo Satellite Metadata. URL: https://www.gsc-europa.eu/support-to-developers/galileo-satellite-metadata.

Herrmann, S., Finke, F., Lülf, M., Kichakova, O., Puetzfeld, D., Knickmann, D., List, M., Rievers, B., Giorgi, G., Günther, C., Dittus, H., Prieto-Cerdeira, R., Dilssner, F., Gonzalez, F., Schönemann, E., Ventura-Traveset, J., Lämmerzahl, C., 2018. Test of the Gravitational Redshift with Galileo Satellites in an Eccentric Orbit. Phys. Rev. Lett. 121, 231102. https://doi.org/10.1103/PhysRevLett.121.231102.

Hoque, M.M., Jakowski, N., Orús-Pérez, R., 2019. Fast ionospheric correction using Galileo Az coefficients and the NTCM model. GPS Solut. 23, 41. https://doi.org/10.1007/s10291-019-0833-3.

Huang, G., Cui, B., Xu, Y., Zhang, Q., 2019. Characteristics and performance evaluation of Galileo on-orbit satellites atomic clocks during 2014–2017. Adv. Space Res. 63, 2899–2911. https://doi.org/10.1016/j.asr.2018.01.034.

Jeanmaire, A., Rochat, P., Emma, F., 1999. Rubidium Atomic Clock for Galileo, in: Proceedings of the 31th Annual Precise Time and Time Interval Systems and Applications Meeting, Dana Point, California. pp. 627–636.

Johnston, G., Riddell, A., Hausler, G., 2017. The International GNSS Service, in: Teunissen, P.J., Montenbruck, O. (Eds.), Springer Handbook of Global Navigation Satellite Systems. Springer International Publishing, Cham. Springer Handbooks, pp. 967–982. https://doi.org/10.1007/978-3-319-42928-1_33.

Koivula, H., Kuokkanen, J., Marila, S., Tenhunen, T., Häkli, P., Kallio, U., Nyberg, S., Poutanen, M., 2012. Finnish permanent GNSS network: From dual-frequency GPS to multi-satellite GNSS, in: 2012 Ubiquitous Positioning, Indoor Navigation, and Location Based Service (UPINLBS), pp. 1–5. https://doi.org/10.1109/UPINLBS.2012.6409771.

Lutz, S., Meindl, M., Steigenberger, P., Beutler, G., Sośnica, K., Schaer, S., Dach, R., Arnold, D., Thaller, D., Jäggi, A., 2016. Impact of the arc length on GNSS analysis results. J. Geod. 90, 365–378. https://doi.org/10.1007/s00190-015-0878-1.

Marquis, W., Krier, C., 2000. Examination of the GPS Block IIR Solar Pressure Model. In: Proceedings of the 13th International Technical Meeting of the Satellite Division of The Institute of Navigation (ION GPS 2000), Salt Palace Convention Center Salt Lake City, UT. pp. 407–415.

Mattioni, L., Belloni, M., Berthoud, P., Pavlenko, I., Schweda, H., Wang, Q., Rochat, P., Droz, F., Mosset, P., Ruedin, H., 2002. The Development of a Passive Hydrogen Maser Clock for the Galileo Navigation System. In: Proceedings of the 34th Annual Precise Time and Time Interval Systems and Applications Meeting, Reston, Virginia, December 2002. pp. 161–170.

Mendonca, M., White, R.M., Santos, M.C., Langley, R.B., 2018. Assessing GPS plus Galileo Precise Point Positioning Capability for Integrated Water Vapor Estimation. In: Freymueller, J.T., Sanchez, L. (Eds.), International Symposium on Earth and Environmental Sciences for Future Generations, volume 147. Springer International Publishing Ag, Cham, pp. 287–292. https://doi.org/10.1007/1345_2016_227.

Montenbruck, O., Dach, R., Steigenberger, P., 2018. New Constellations for Geodesy: The IGS Multi-GNSS Pilot Project (MGEX), Presentation at The Symposium of the IAG Subcommission for Europe (EUREF), 30 May - 01 June 2018. The Netherlands, Amsterdam.

Montenbruck, O., Schmid, R., Mercier, F., Steigenberger, P., Noll, C., Fatkulin, R., Kogure, S., Ganeshan, A., 2015. GNSS satellite geometry and attitude models. Adv. Space Res. 56, 1015–1029. https://doi.org/10.1016/j.asr.2015.06.019.

Montenbruck, O., Steigenberger, P., Prange, L., Deng, Z., Zhao, Q., Perosanz, F., Romero, I., Noll, C., Stürze, A., Weber, G., Schmid, R., MacLeod, K., Schaer, S., 2017. The Multi-GNSS Experiment (MGEX) of the International GNSS Service (IGS) – Achievements,

prospects and challenges. Adv. Space Res. 59, 1671–1697. https://doi.org/10.1016/j.asr.2017.01.011.

Nicolini, L., Caporali, A., 2018. Investigation on Reference Frames and Time Systems in Multi-GNSS. Remote Sens. 10, 80. https://doi.org/10.3390/rs10010080.

Pearlman, M.R., Degnan, J.J., Bosworth, J.M., 2002. The International Laser Ranging Service. Adv. Space Res. 30, 135–143. https://doi.org/10.1016/S0273-1177(02)00277-6.

Prange, L., Arnold, D., Dach, R., Schaer, S., Sidorov, D., Stebler, P., Villiger, A., Jäggi, A., 2018. CODE product series for the IGS-MGEX project. URL: http://www.aiub.unibe.ch/download/CODE_MGEX, doi:10.7892/boris.75882.2. library Catalog: boris.unibe.ch Publisher: Astronomical Institute, University of Bern.

Prange, L., Beutler, G., Dach, R., Arnold, D., Schaer, S., Jäggi, A., 2020. An empirical solar radiation pressure model for satellites moving in the orbit-normal mode. Adv. Space Res. 65, 235–250. https://doi.org/10.1016/j.asr.2019.07.031.

Prange, L., Orliac, E., Dach, R., Arnold, D., Beutler, G., Schaer, S., Jäggi, A., 2017a. CODE's five-system orbit and clock solution–the challenges of multi-GNSS data analysis. J. Geodesy 91, 345–360. https://doi.org/10.1007/s00190-016-0968-8.

Prange, L., Villiger, A., Sidorov, D., Dach, R., Schaer, S., Beutler, G., Susnik, A., Jäggi, A., 2017b. Impact of new background models on GNSS orbit determination, in: 6th international Colloquium - Scientific and Fundamental Aspects of GNSS/Galileo, Valencia, Spain. https://doi.org/10.7892/boris.112418.

Rochat, P., Gioia, M., 2016. Next generation atomic clocks, Presentation at Stakeholder workshop on EU Space Work Programme 2018–2020, Radisson Blu Royal Hotel, Rue du Fossé aux Loups 47. Belgium, Brussels.

Schönemann, E., Springer, T., Dilssner, F., Garcia, C., Flohrer, C., Reichel, F., Enderle, W., Zandbergen, R., 2015. Precise Orbit Determination for GNSS satellites, Presentation at 5th International Colloquium - Scientific and Fundamental Aspects of the Galileo Programme, Braunschweig, Germany. p. 20. URL: http://navigation-office.esa.int/attachments_12649499_1_070_schoenemann.pdf.

Sirikan, N., Côme, H., Stojković, I., Ventura-Traveset, J., Lucas, R., Falcone, M., 2018. Galileo 5 and 6 Eccentric Satellites: Mission Recovery and Exploitation Part I. InsideGNSS 2018 (July/August), 38–47.

Sośnica, K., Bury, G., Zajdel, R., 2018. Contribution of Multi-GNSS Constellation to SLR-Derived Terrestrial Reference Frame. Geophys. Res. Lett. 45, 2339–2348. https://doi.org/10.1002/2017GL076850.

Sośnica, K., Bury, G., Zajdel, R., Strugarek, D., Drożdżewski, M., Kazmierski, K., 2019. Estimating global geodetic parameters using SLR observations to Galileo, GLONASS, BeiDou, GPS, and QZSS. Earth, Planets and Space 71, 20. https://doi.org/10.1186/s40623-019-1000-3.

Springer, T.A., Beutler, G., Rothacher, M., 1999. A new solar radiation pressure model for GPS satellites. GPS Solut. 2, 50–62. https://doi.org/10.1007/PL00012757.

Steigenberger, P., Montenbruck, O., 2017. Galileo status: orbits, clocks, and positioning. GPS Solut. 21, 319–331. https://doi.org/10.1007/s10291-016-0566-5.

Ventura-Traveset, J., 2017. GNSS/GALILEO a major opportunity for science, Presentation at 6th Galileo Science Colloquium - Scientific and Fundamental Aspects of GNSS/Galileo. Valencia, Spain.

Wang, N., Li, Z., Li, M., Yuan, Y., Huo, X., 2018. GPS, BDS and Galileo ionospheric correction models: An evaluation in range delay and position domain. J. Atmos. Solar Terr. Phys. 170, 83–91. https://doi.org/10.1016/j.jastp.2018.02.014.

Wielgosz, P., Hadaś, T., Klos, A., Paziewski, J., 2019. Research on GNSS positioning and applications in Poland in 2015–2018 https://doi.org/10.24425/gac.2019.126089.

Zhang, P., Tu, R., Gao, Y., Liu, N., Zhang, R., 2019. Evaluation of carrier-phase precise time and frequency transfer using different analysis centre products for GNSSs. Meas. Sci. Technol. 30, 065003. https://doi.org/10.1088/1361-6501/ab0f7f.

Zhang, P., Tu, R., Zhang, R., Gao, Y., Cai, H., 2018. Combining GPS, BeiDou, and Galileo Satellite Systems for Time and Frequency Transfer Based on Carrier Phase Observations. Remote Sens. 10, 324. https://doi.org/10.3390/rs10020324.

Please cite this article as: D. Sidorov, et al., Adopting the empirical CODE orbit model to Galileo satellites, Advances in Space Research, https://doi.org/10.1016/j.asr.2020.05.028